Distribution of Impurities, Alloying and Binder Elements in Rutile (TiO_{2-x}) Scales at High-Temperature Oxidation

V.B. Voitovich

Institute for Problems of Materials Science, 252680, GSP. Kiev-180
Krzhyzhanovsky Str. 3, Ukraine

NOMENCLATURE

D	diffusion coefficient, m^2s^{-1}
$D_{\|c}$	diffusion coefficient in direction parallel to crystallographic axis *c*, m^2s^{-1}
$D_{\perp c}$	diffusion coefficient in direction perpendicular to crystallographic axis *c*, m^2s^{-1}
P_o	oxygen partial pressure, Pa
r_{cat}	radius of cation, nm
r_{chan}	radius of channel, nm
Me_{Ti}	impurity cation in a normal lattice site
$V^{\cdot\cdot}_o$	oxygen vacancy
O_{xo}	oxygen atoms in a normal lattice site
Ti^x_{Ti}	titanium cation in a normal lattice site
$Ti^{\cdot\cdot\cdot\cdot}$	interstitial titanium cation
ΔG	Gibbs free energy, kJ/mol
e'	electrons in the conduction band

ABSTRACT

The distribution and redistribution of impurities, alloying elements and components of binders in the rutile (TiO_{2-x}) scales during high-temperature oxidation of titanium, titanium alloys, refractory compounds of titanium (carbide and diboride) and materials based on them have been studied by SEM, EPMA and XRD methods. The correlation between defect and crystallographic structures of rutile with diffusion processes in the scales and redistribution of elements at the matrix/scale, scale/scale and scale/gas interfaces is ascertained. Mechanisms of diffusion processes in scales during high-temperature oxidation are discussed.

Key words: diffusion, rutile, scale, oxidation, distribution of elements, titanium

1. INTRODUCTION

The mechanism of interaction of metals, alloys and refractory compounds with gaseous atmospheres determines their heat and oxidation resistance. High-temperature oxidation of materials has been the subject of numerous investigations of chemical, physical and structural aspects. Impurities and alloying elements have a pronounced effect on the structure and phase composition of both scales and starting materials, and the oxidation kinetics are different. The behaviour of these processes has been studied to a limited extent only. Oxidation is a complex and manifold process /1/. In studies of diffusion processes in scales it is necessary to take into account such factors as oxidation kinetics, thermodynamics, phase compositions and structures both of starting materials and scales, morphology and crystallographic structure of oxides, sintering of scales, stresses in the scale, etc.

Study of the high-temperature oxidation of titanium-based alloys and refractory compounds of titanium is of specific interest due to their wide application in industry. Titanium dioxide, TiO_{2-x}, (rutile modification) forms a bulk of scales at temperatures above 700°C /2/. The defect and crystallographic structures of rutile establish specific peculiarities of diffusion processes both in the scales and at the matrix/scale or scale/gas interfaces. A study of these regularities is the main objective of the present investigation.

2. EXPERIMENTAL

The alloy compositions were evaluated by wet chemical analysis. The samples of the alloys were oxidized in the temperature range of 600-1200°C in air. The structure of the oxidized samples and distribution of the elements were investigated on the cross-sections, prepared by the conventional metallographic technique. The brittle scales were blocked up by an acryl monomer. The scale morphology and structure of the oxidized samples were studied by scanning electron microscopy (SEM) with a microanalyzer JCXA-733. Both the secondary electron image (SEI) and the back-scattered electron image (BEI) were used. Specimens were gold-sputtered for SEM and EPMA investigations by cathode sputtering with a JFC-1100 unit. The phase composition of the oxidized products was examined by X-Ray diffraction (XRD). An X-Ray diffractometer DRON-3 with a CuK_α source was used. Chemical heterogeneities and the distribution of some elements both in the scales and in the alloy matrix were investigated by electron probe microanalysis (EPMA) with a microanalyzer JCXA-733. Microhardness was measured with a PMT-3 unit, the indenter loading being 0.2N.

3. MATERIALS

Ti-2% Fe ingots were produced in a vacuum-arc furnace and annealed at 1000°C for 50 hr under vacuum. The specimens for TGA measurements were 5 mm in diameter and 10 mm in length. Refractory materials (TiC, TiB_2) and hard metals were manufactured by the powder metallurgy route. Chemical compositions are listed in Table 1. Specimens were 7 x 7 x 7 mm in size. All sides were preliminarily ground. Starting structures were controlled by EPMA and SEM methods.

4. RESULTS AND DISCUSSION

4.1. Defect and Crystallographic Structures of Rutile (TiO_{2-x})

Crystallographic and defect structures of oxides establish both protective properties of scales and the mechanism of diffusion of impurities and alloying elements in scales since diffusion is controlled by point defects.

Rutile (TiO_{2-x}) has a tetragonal lattice with parameters a = 0.4593 nm and c = 0.2959 nm /3/. The structure of rutile has been adequately described /3-6/. Channels with low values of electron density are the main specific feature of the rutile structure. These channels are formed by TiO_6 octahedra in a TiO_2 lattice (Fig. 1). The distribution of potential energy in rutile lattice was determined and calculated by Yagi *et al.* /6/. This investigation lends support to the validity of the initial assumptions /4/ as to low values of electron energy density. The radius of the channels is 0.077 nm on average /7,8/. This makes diffusion of cations along channels theoretically feasible, provided that cation radii are less than 0.077 nm. Values of the cation radii in oxides are associated with the nature of "metal-oxygen" chemical bonds and the value of the coordination number /9/.

Rutile (TiO_{2-x}) is a n-type semiconductor with oxygen deficiency /4,5/. Anionic vacancies $V^{\cdot\cdot}_o$ and interstitial cations (Ti^{3+}, Ti^{4+}) /4,5/ are the main point defects of rutile lattice. There are at least three models

Table 1

Chemical Composition of the Alloys

Alloy	Content of Elements, wt %															
	C	N	O	B	Cu	Mg	Ca	Al	Si	Cr	Mo	W	Co	Fe	Ni	Ti
Ti-2%Fe	0.05	0.03	0.12	-	0.01	0.02	-	0.13	0.02	0.05	-	-	-	2.06	0.02	97.49
TiC-Ni-Mo*	13.8	0.37	0.82	-	0.04	-	0.02	0.01	0.01	0.05	5.31	1.90	0.20	0.73	15.90	60.67
TiB_2 (impure)	0.28	0.10	0.31	30.4	0.01	0.27	0.03	0.08	0.05	0.02	0.72	0.11	0.04	1.78	1.37	64.43
$(Ti,Cr)B_2$-Cu-Ni	0.35	0.08	0.45	18.80	24.35	0.08	0.05	-	0.06	6.04	-	0.12	0.03	0.85	12.20	36.54
TiC-Ni-Cr**	13.9	0.21	1.16	-	0.03	-	0.01	-	0.02	4.18	-	1.30	0.22	0.65	14.85	63.47

* - 0.08% of free carbon;
** - 0.05% of free carbon.

Me_2O_3-type oxide dissolves in TiO_2 lattice with substitution of titanium cations in the lattice site, and provided that oxygen vacancies are dominant defects, the dissolution will be described by the equation (1)

$$Me_2O_3 <=> 2\,Me_{Ti} + V^{\cdot\cdot}_o + 3O^x_o \quad (1)$$

In this case, dissolution of impurity cations increases the concentration of anion vacancies. If titanium interstitial cations are dominant defects, dissolution will be described by the equations (2) and (3)

$$2Me_2O_3 + TiO_2 <=> 4Me_{Ti} + Ti^{\cdot\cdot\cdot\cdot} + 8O^x_o \quad (2)$$

$$e' + 2Me_2O_3 + TiO_2 <=> 4Me_{Ti} + Ti^{\cdot\cdot\cdot} + 8O^x_o \quad (3)$$

In such a manner, the concentration of interstitial titanium cations will be increased. Electroneutrality /14/ requires that:

$$[Me_{Ti}] + [e'] = 4[Ti^{\cdot\cdot\cdot\cdot}] + 3[Ti^{\cdot\cdot\cdot}] + 2[V^{\cdot\cdot}_o] \quad (4)$$

Cations of impurities with a valency higher than +4 have the opposite effect /3,4,13,20/.

A concentration of defects in rutile lattice influences the diffusion coefficients. It has an appreciable effect on the oxidation of titanium-based materials, when scale consists of rutile. The diffusion of titanium cations in rutile is accelerated in the presence of impure cations with a low valency /17/.

An intensive sintering of scale starts at temperatures above 1000°C /21-24/ and the density of rutile may be as much as 94-99% compared with the theoretical one. The grain size of rutile is increased with temperature rise. Diffusion processes and grain-boundary diffusion play a dominant role at temperatures for grains with size exceeding 1 μm /24-26/. Grain-boundary diffusion increases the rate of rutile sintering /25,26/. Impurities promote sintering of rutile /21/ as a result of intensification of rutile crystallite growth preceding sintering (NiO, Fe_2O_3), increasing of concentration of anion vacancies and formation of liquid phase. Diffusion of oxygen is a rate-controlling stage of rutile sintering /27/. Formation of the liquid phase in scale during oxidation of titanium alloys, refractory compounds and hard metals is unlikely.

Diffusion of oxygen in the polycrystalline rutile has not yet been studied. Results of investigations of oxygen diffusion in TiO_2 single crystals are in close agreement and their values are $D = 10^{-18}$ m^2s^{-1} at 1000°C /28/. Bagshaw and Hyde /29/ pointed out the possibility of an accelerated diffusion of oxygen along the grain boundaries. Circumstantial evidence /3,27/ indicates that the rate of oxygen diffusion in a scale is less than for titanium.

4.2. Redistribution of Elements in TiO_2 Scales

The values of the Gibbs free energy (ΔG) of oxidation reactions of the majority of metals, except for Zr, Al, Ca and Mg, are lower than for titanium /30/. Rutile (TiO_{2-x}) is the most stable titanium oxide and forms a base of scales. It specifies the formation of different oxides and the possibility of their redistribution both in the scale and of the matrix/scale and scale/gas interfaces during oxidation.

In parallel with the general regularities, governed by thermodynamics and rutile structure, there are specific features, defined by oxidation mechanisms and the structure of individual materials. The oxidation behaviour of some of these materials will be discussed in the following sections. Only diffusion processes in the scales and at the interfaces will be discussed. Diffusion processes in the matrix of materials will not be discussed here, because they are not the subject of the present investigation.

4.2.1. Oxidation of titanium and its alloys

Oxidation of titanium and titanium-based alloys shows some peculiarities, such as a significant solubility of oxygen, (α + β) - binary phase structure placed under the scale at temperatures above 900°C, and the formation of multilayered scale /2/. Oxygen stabilizes the α-phase and increases its electron concentration /31/. This phenomenon along with a low solubility of impurities and alloying elements in the α-phase with HCP lattice facilitates their diffusion into the metallic matrix during oxidation. In the binary phase (α + β)-region the majority of alloying elements are concentrated mainly in the β-phase with BCC-lattice. A high rate of diffusion of alloying elements and impurities causes the high concentration of oxygen

in α-phase wedges /32/.

Impurities in titanium or alloying elements in alloys /33,34/ may diffuse into both the inner and the outer scales and into the metallic matrix from the zone of oxygen solid solution in α-titanium.

The basic diffusion processes are:

a) Enrichment of the metal/scale interface in alloying elements due to preferred diffusion of titanium cations into the scale during oxidation;
b) Diffusion of some impurity cations into the scale at high temperatures (above 1000°C), and variation in the concentration of point defects in rutile lattice and possible enrichment of scale/gas interface in some impurities and alloying elements;
c) Diffusion of elements from the HCP-lattice of an α-solid solution of oxygen in titanium into grains of the β-phase with BCC-lattice at temperatures above 900°C.

Peculiarities of a redistribution of elements are determined by the rate of impurity diffusion both in the titanium /35/ and in the rutile /15/, Ti-Me binary alloy phase diagrams /36/, values of the free energy of Me_xO_y formation /2,30/, effect of impurities on the electron concentration of the alloys /31,37/, solubility of elements in the α- and β-titanium /2,36/ and sintering of scale /2/.

Regularities of these processes have been demonstrated with Ti-2% Fe alloy oxidized at 1000°C for 7 hr. The structure of the oxidized alloy is shown in Fig. 2. The scale consists of two layers of rutile (Fig. 2b). The outer layer is more sintering in comparison with the inner one. The smooth layer (Fig. 2c) with a microhardness value close to 1 GPa at the matrix/scale interface is a solid solution of oxygen in the α-titanium. Distribution of iron Fe K_α (Fig. 2d) is not coincident with this layer. Iron forms a diffusion barrier immediately ahead of the zone of a solid solution. Enrichment of these regions in iron is caused by its diffusion from the α-solid solution of oxygen into the matrix of the alloy during oxidation due to an increased electron concentration in the α-phase /37/. There are no visible changes in the distribution of iron at the inner scale/outer scale interface (Fig. 2e,f). The peak + background/background ratio for the Fe K_α-radiation averages between 4 and 9 and the distribution of iron is homogeneous. Later, a certain part of the iron cations diffuses from the inner scale into the outer scale in combination with titanium and promotes the sintering of scales, and the outer layer is essentially sintered. The regularities of diffusion of some impurity cations /15/ facilitate their fast diffusion in rutile. This determines the formation of the diffusion barrier at the scale/gas interface (Fig. 2h) with time, although values of Gibbs energy for iron oxidation are lower than for titanium /30/. Iron cations form an irregular zone at the scale/gas interface (Fig. 2b). These regularities are also valid for other Ti-Me systems (Me = Co, Si, Ni, Cu, Cr, Mn) /2,3,32/. This is determined by preferential oxidation of titanium /2/ and by mechanisms of diffusion of transition metal cations in rutile /15/.

During oxidation of titanium-aluminum alloys the scale consists of both TiO_2 and Al_2O_3 oxides /38-40/. Initial formation of an internal Al_2O_3 layer takes place at high temperatures and at a sufficient concentration of aluminum in the starting alloy.

4.2.2. Oxidation of titanium carbide cermets

Cubic carbides of transition metals with the NaCl-type structure are characterized by a wide region of homogeneity. These carbides have filled-up sites only in the carbon sublattice /41/.

The substitution of carbon by oxygen during oxidation of carbides leads to the formation of an intermediate oxycarbide solution with a cubic lattice and vacancies in both sublattices /42,43/ due to a reinforcement of the oxygen screening action on the metal/metal interaction in comparison with the carbon /44/. Formation of vacancies in the metallic sublattice is determined by the tendency to conserve a constant value of valence electrons accounted for by a pair of sites of elementary cells in consistent phases of intermediate compositions /45/. These features determine the significant role of titanium cations in the formation of a two-layered scale /42,46,47/. The outer layer is formed over the original surface of titanium carbide /46/. The inner layer is formed due to the dissolution of oxygen /42/. At temperatures above 800°C, part of the oxide layer, which is formed as a result of oxygen ion diffusion, is reduced. Simultaneously with this process the thickness of a layer, formed due to diffusion of titanium cations, is increased /46/.

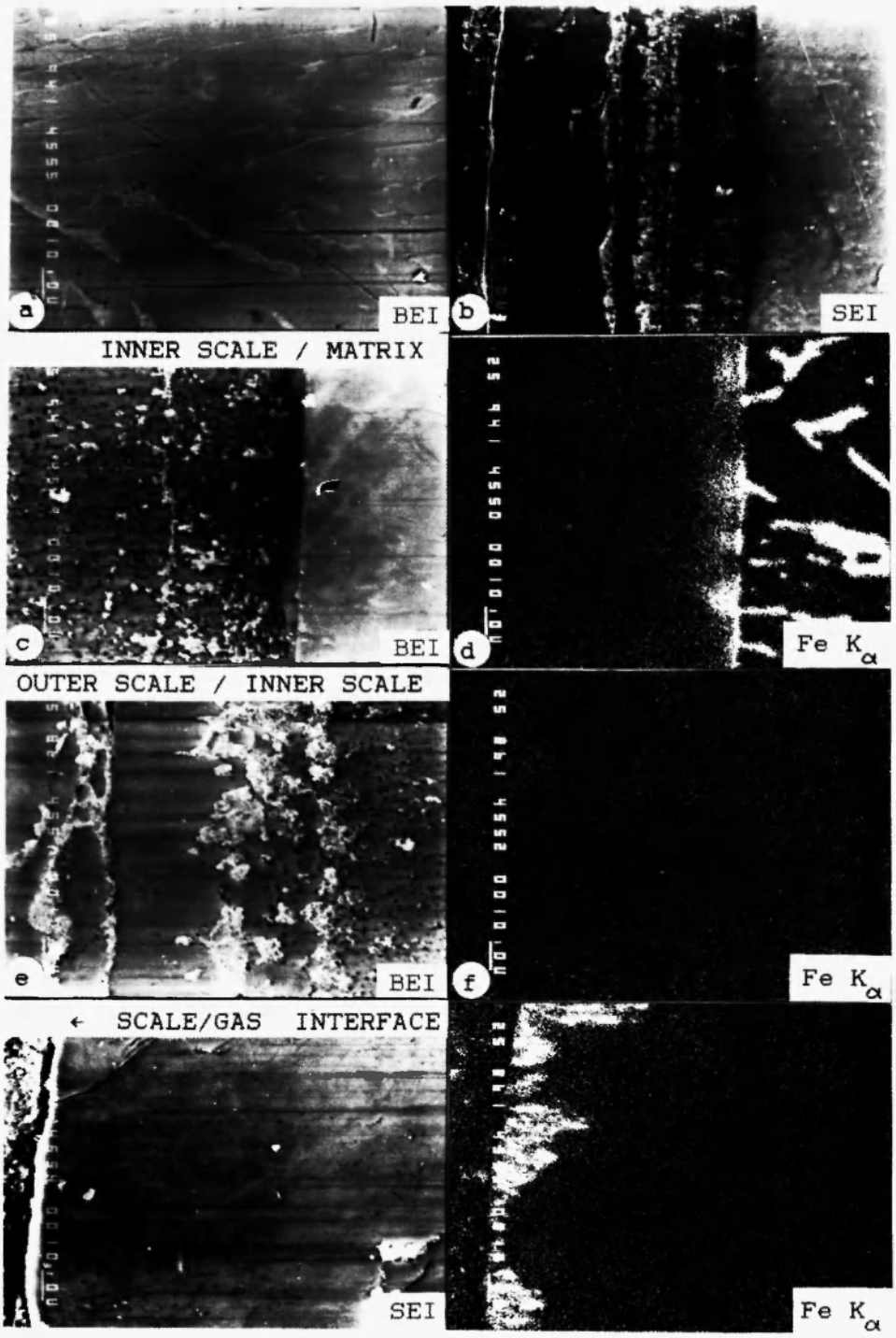

Fig. 2: Structure of the oxidized alloy Ti-2%Fe (1000°C, 7 hr); a – starting alloy; b – structure of scale, general view; c – matrix/inner scale interface; d – Fe K_α radiation; e – inner scale/outer scale interface; f – Fe K_α radiation; g – outer scale/gas interface; h – Fe K_α -radiation.

The general regularities of distribution of elements were investigated for oxidation of the TiC-Ni-Mo alloy, and similar regularities were established during oxidation of the TiC-Ni-Cr alloy as well /48/. These alloys have a specific structure of carbide grains /49/. There are three main structural components in these alloys. They are TiC-core, (Ti,Mo)C or (Ti,Cr)C-rim and Ni-Mo or Ni-Cr binder which also contains such elements as Fe, Co, Cr, Si (Fig. 3b). The structure of the scale on TiC-Ni-Mo alloy oxidized at 1200°C for 6 hr is shown in Fig. 3. A two-layered scale is formed (Fig. 3a,c-e). The structures and phase compositions of the outer and the inner layers are different.

The inner layer, like the outer one, consists of rutile. There are fine-grained (0.5-10 μm in size), uniformly distributed inclusions of oxidized binders in the inner layer (Fig. 3d). They were identified as NiO, $NiMoO_4$, $NiCrO_3$, $Ni_xTi_{1-x}O$ phases. This type of structure of the inner layer is determined by an oxygen solution in the carbide during oxidation.

This process is shown schematically in Fig. 4. Inclusions of oxidized binder coarsen and coagulate

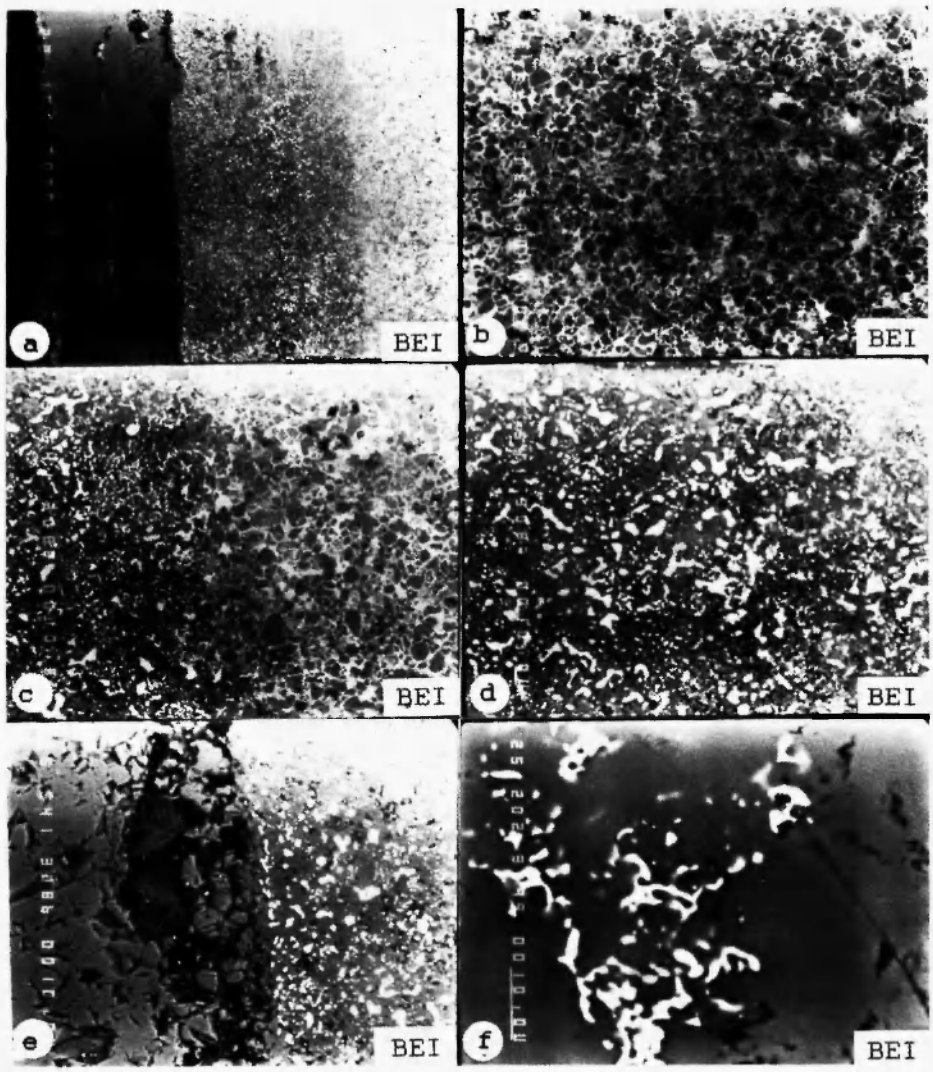

Fig. 3: Structure of the oxidized alloy TiC-Ni-Mo (1000°C, 56 hr); a – general view of the two-layered scale; b – matrix of the alloy; c – matrix/inner scale interface; d – inner scale; e – inner scale/outer scale interface; f – outer layer.

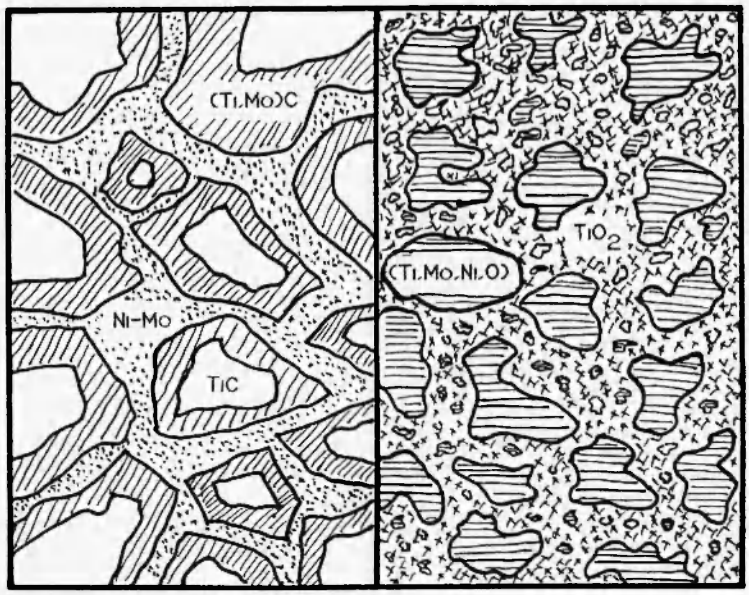

Fig. 4: Scheme of mechanism of formation of the inner scale in TiC-Ni-Mo alloy; a – starting alloy; b – inner layer of scale.

with time. The titanium content in the oxidized binder (approximately 1.5%) differs from that of the binder of starting hard metals (up to 9%). The titanium content in the binder decreases through its diffusion into the adjacent scale and subsequent diffusion into the outer scale. Molybdenum diffuses from the (Ti,Mo)C-rim into inclusions of the oxidized Ni-Mo binder and is content in the scale is low. These inclusions are not present in the outer scale.

The formation of two-layered scale determines the redistribution of basic components of hard metals, i.e., titanium, nickel and molybdenum, at the matrix/scale, inner scale/outer scale and scale/gas interfaces. There are no pronounced variations of redistribution at the matrix/scale interface. This is determined by features of the oxidation mechanism as a result of oxygen dissolution.

The distribution of Ti, Ni, and Mo at the inner scale/outer scale interfaces is shown in Fig. 5. Nickel forms a virtually solid chain of inclusions (Fig. 5c), whereas the Mo L_α intensity in this inclusion is low (Fig. 5d). The intensity of Mo L_α radiation in the scale, except for inclusions of the oxidized binder, is close to that of the background. The distribution of impurities of binder (Fe, Co, Cr) at this interface is similar to that for nickel. However, their content in both the starting hard metal and in the scale is insignificant.

Some of the cations of impurities and alloying elements diffuse into the outer scale (Fig. 6) in combination with titanium cations. In accordance with EPMA, a 7 μm thick diffusion barrier (Fig. 6a,c) is formed by nickel, iron and cobalt. The distribution of iron and nickel is shown in Fig. 6b,c. Iron is an impurity in the Ni-Mo binder and its distribution is identical. The values of the peak+background/ background ratio for Ni K_α and Fe K_α - radiation at a distance of 5 μm from this diffusion barrier exceed the background values insignificantly.

The formation of diffusion barriers at the scale/gas interface is determined by both the chemical affinity of the elements to oxygen /2/ and the diffusion mobility of their cations in rutile /15/. The first factor determines preferential formation of some oxides in scale. The diffusion mobility determines the rate of diffusion of cations in rutile and the likelihood of a later redistribution of elements. Such elements as cobalt, nickel and iron with the lowest values of chemical affinity to oxygen among the elements of hard metal (Ti, Mo, Ni, Si, Fe, Co, Cr), and with a high diffusion mobility in rutile /15/, diffused into the scale/ gas

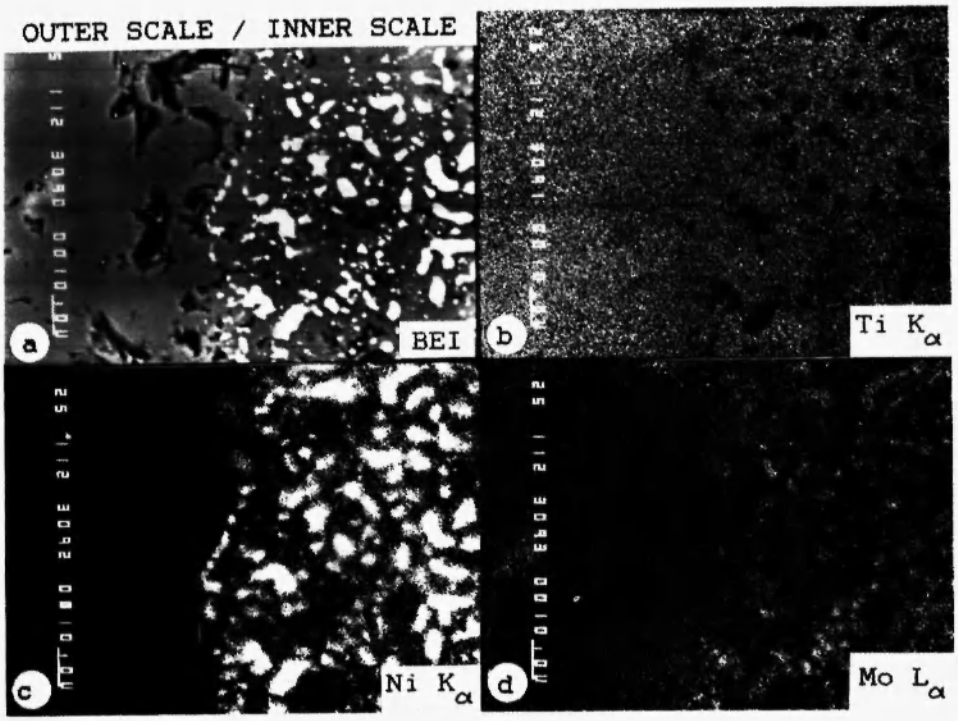

Fig. 5: Redistribution of Ti, Ni and Mo at the inner scale/outer scale interface in the TiC-Ni-Mo alloy; a – backscattered electrons; b – Ti K_α; c – Ni K_α; d – Mo K_α -radiation.

interface since higher values of oxygen partial pressure are necessary for its oxidation. Molybdenum and silicon with higher values of (ΔG) as compared to nickel, iron and cobalt, but with a lower diffusion mobility, were not found in the rutile of the outer scale.

Defects of the scale form a diffusion barrier (Fig. 6d-f), hindering the diffusion of impurity elements into rutile /7,16/.

The regularities of oxidation of titanium nitride /47/ are similar to titanium carbide oxidation. Therefore, the foregoing regularities must be correct for TiN-based alloys.

4.2.3. Oxidation of titanium diboride

The distribution of alloying elements and impurities during titanium diboride oxidation has not been adequately studied /50,51/. The formation of a two-layered scale, in accordance with the above-mentioned regularities for titanium carbide oxidation, has not occurred. An inner layer of scale has not been formed.

In the Ti-B-O system /52/, rutile (TiO_2) is stable at partial pressures of oxygen close to atmospheric ones and the partial pressure of B_2O_3 above 10^{-9} Pa. Other oxides of titanium are stable only at a low partial pressure of oxygen /52/. The main products of oxidation of titanium diboride are TiO_2 and B_2O_3. At temperatures above 700-800°C, titanium dioxide presents only a high-temperature modification, i.e., rutile is formed.

With a temperature rise above 950°C, a fraction of B_2O_3 decreases as a result of intensive evaporation /53/, and B_2O_3 concentrates in the outer layers /53/.

The distribution of elements at the matrix/scale interface in the impure (Fe, Ni, Mo, Mg, Cr) titanium diboride oxidized at 1200°C during 5 hr is shown in Fig. 7. The distribution of both titanium, boron (Fig. 7b,c) and impurities (Fig. 7e-h) occurs during oxidation. Impurities are concentrated at the boride/scale interface and diffuse into the scale. Titanium, as an element with a higher chemical affinity to oxygen, is the bulk of the scale. Other elements (Ni, Mo, Fe) are concentrated mainly at the boride/scale interface (Fig. 7e-h). The chemical affinity of magnesium to oxygen is higher than for titanium, and magnesium does not

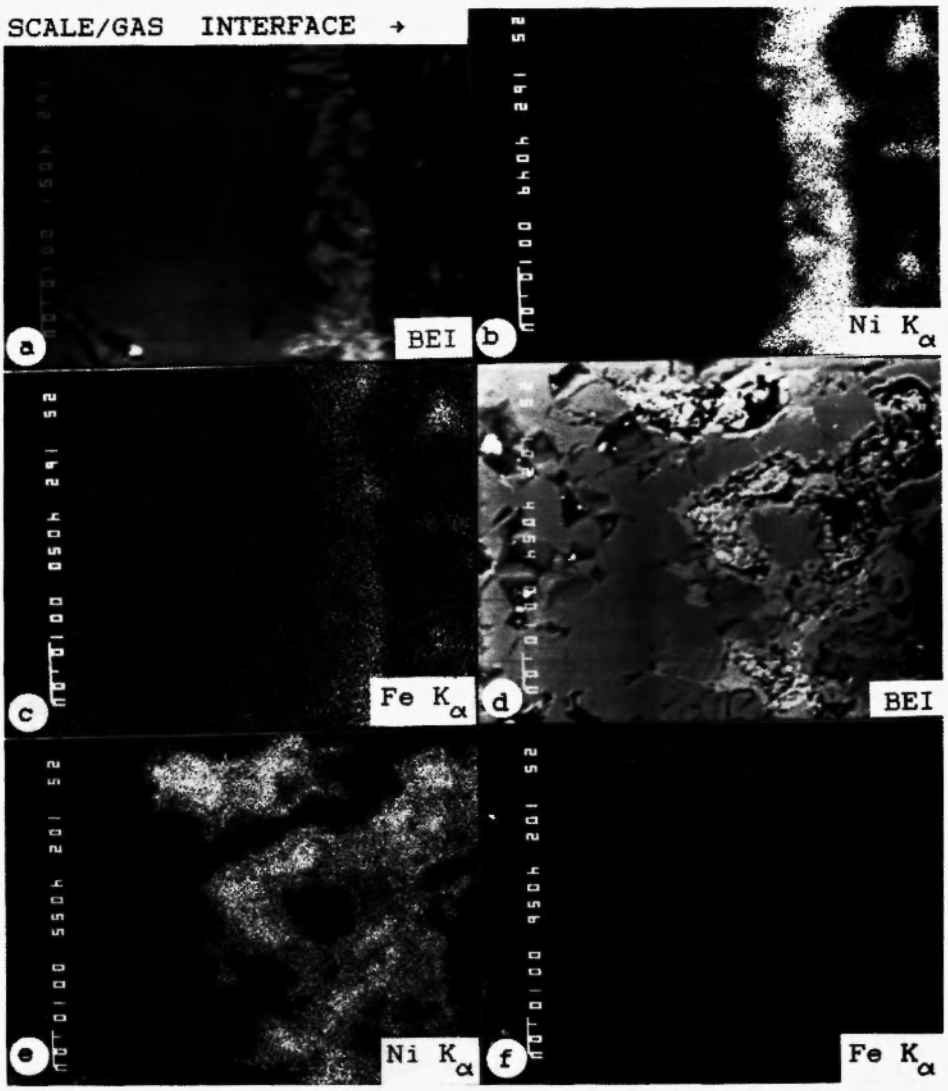

Fig. 6: Diffusion barrier (a-c) at the scale/gas interface and defects in the scale (d-f) on the TiC-Ni-Mo alloy (1000°C, 56 hr); a – backscattered electrons; b – Ni K_α; c – Fe K_α; d – backscattered electrons; e – Ni K_α; f – Fe K_α - radiation.

enrich this interface. Magnesium forms scale either with titanium (Fig. 7f) or, at a sufficient concentration, it forms primarily scale /30/. A light band (Fig. 7a) between the diboride and the scale is a diffusion barrier. It is composed of impurity elements (Fe, Ni, Mo, etc.). Elements with high diffusion mobility in rutile diffuse into the outer layers of scale with time.

By this means, diffusion processes at the boride/ scale interface are determined by values of the Gibbs energy /30/ of the more preferable oxidation reactions of TiB_2 and impurities.

Diffusion of elements in the scale on titanium diboride is determined by values of Gibbs energy, ionic radii and valence of impurity cations /15/. The mechanism for diffusion of impurity cations determines a homogeneity of their distribution in the scale and the possibility of their diffusion in the scale. EPMA investigations of the scale reveal that the concentration of nickel and iron in the 3-5 μm thick outer layers at the scale/gas interface increases. The intensities of X-ray characteristic radiation of these elements sharply increase in this layer while the corresponding values in

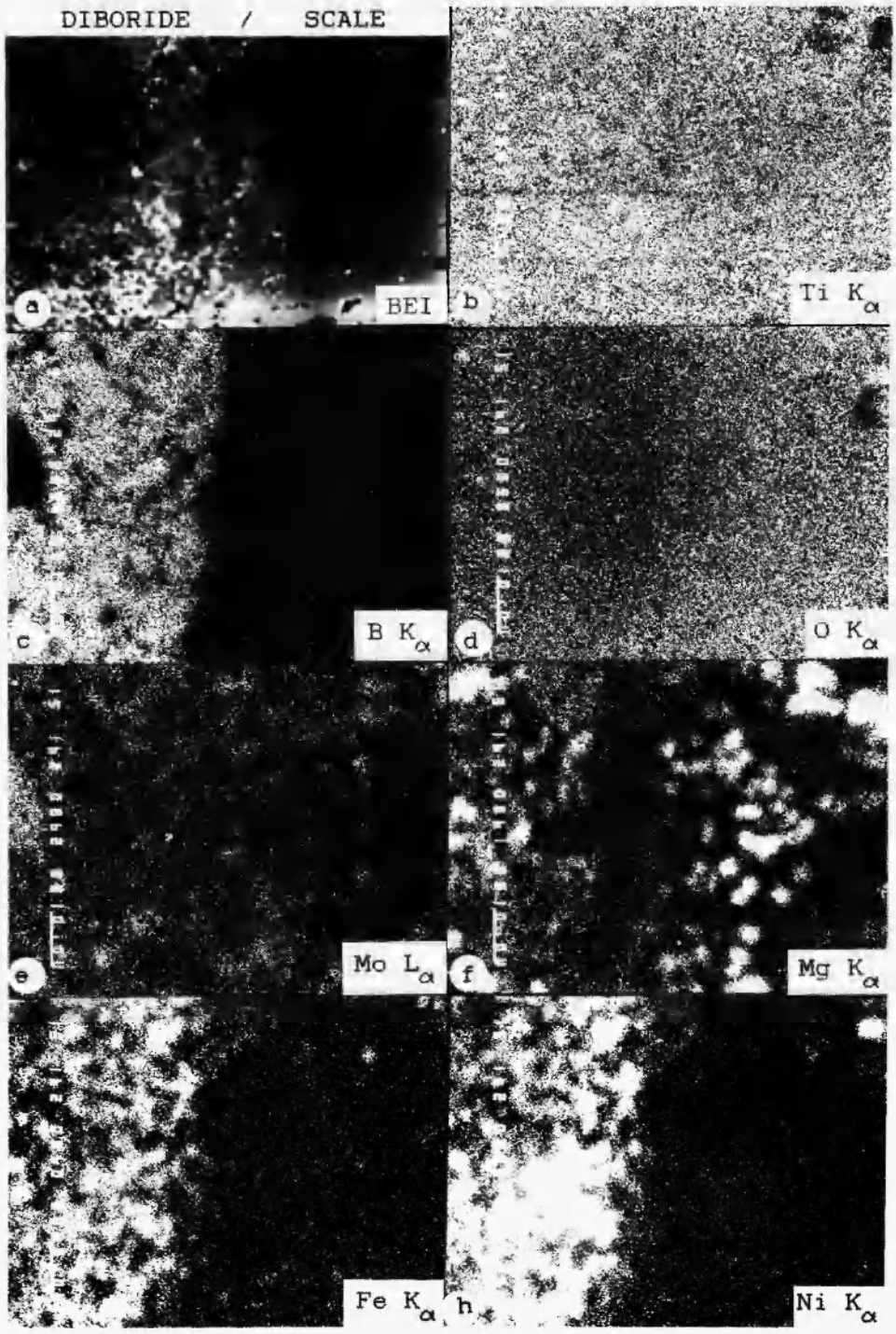

Fig. 7: The matrix scale interface in the titanium diboride with high impurity content (1200°C, 5 hr); a – backscattered electrons; b – Ti K_α; c – B K_α; d – O K_α; e – Mo L_α; f – Mg K_α; g – Fe K_α; h – Ni K_α-radiation.

the scale are close to those of the background /54/. Molybdenum was not found in the outer layers of the scale. The intensity of Mo L_α radiation decreases away from the boride/scale interface (Fig. 7e). This is related to the evaporation of MoO_3 at temperatures above 1000°C and a low diffusion mobility of molybdenum cations in rutile.

The foregoing regularities are also true for the distribution of binder during oxidation of TiB_2-based alloys. The distribution of copper, nickel, chromium and titanium in the (Ti, Cr)B_2-Cu-Ni alloy oxidized at 1200°C for 6 hr is shown in Figs. 8 and 9. These elements form a diffusion barrier at the alloy/scale interface. The first one is predominantly formed by copper and nickel (Fig. 8c,d). The intensity of Ti K_α - irradiation is close to background values, except for some inclusions (Fig. 8e). Chromium is distributed as some inclusions of chromium diboride (Fig. 8f) and does not take part in the formation of this barrier. Nickel, copper and, to some extent, chromium, diffuse in the scale and form a second diffusion barrier at the scale/gas interface with time (Fig. 9). In accordance with the EPMA data, these light crystallites (Fig. 9a,b) are comprised of nickel, copper and chromium (Fig. 9c-

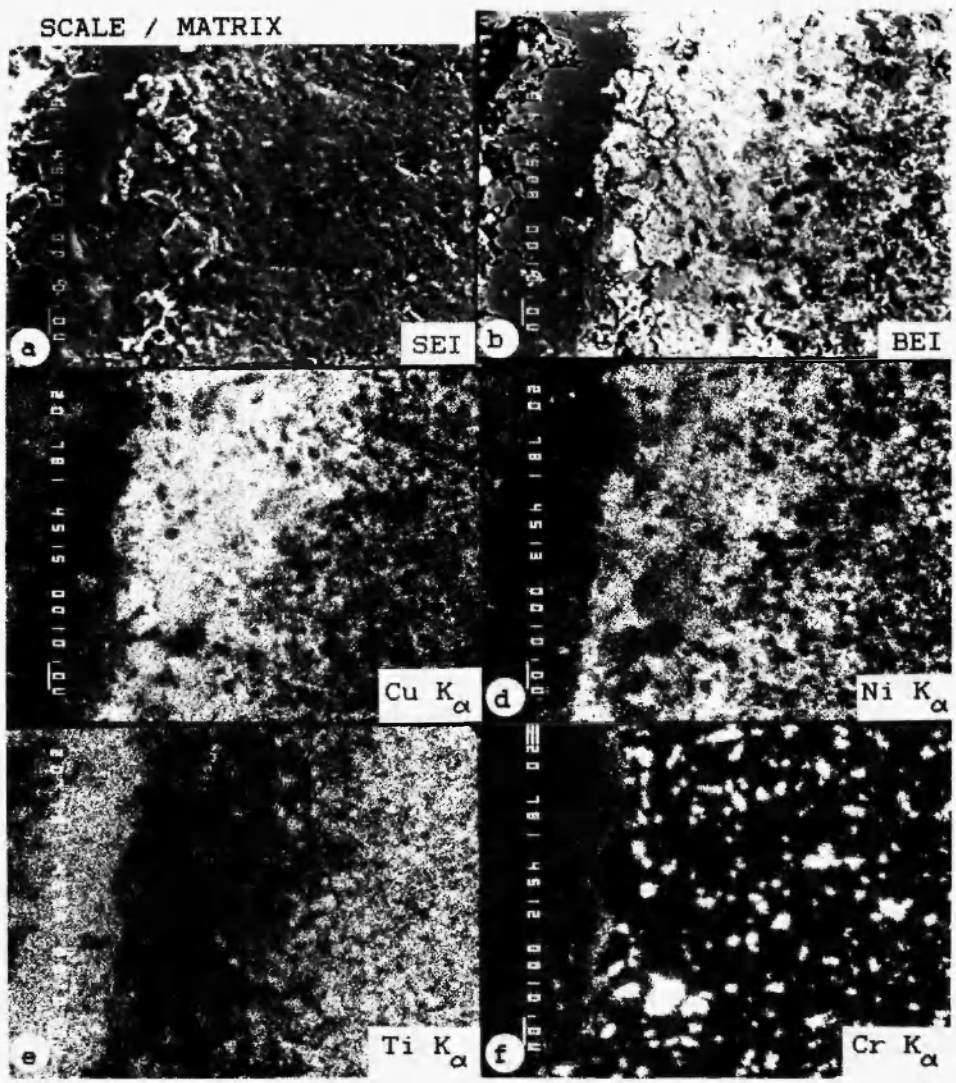

Fig. 8: The matrix/scale interface in the (Ti, Cr)B_2-Cu-Ni alloy (1200°C, 6 hr); a – structure (secondary electrons) b – structure (backscattered electrons); c – Cu K_α; d – Ni K_α; e – Ti K_α; f – Cr K_α-radiation.

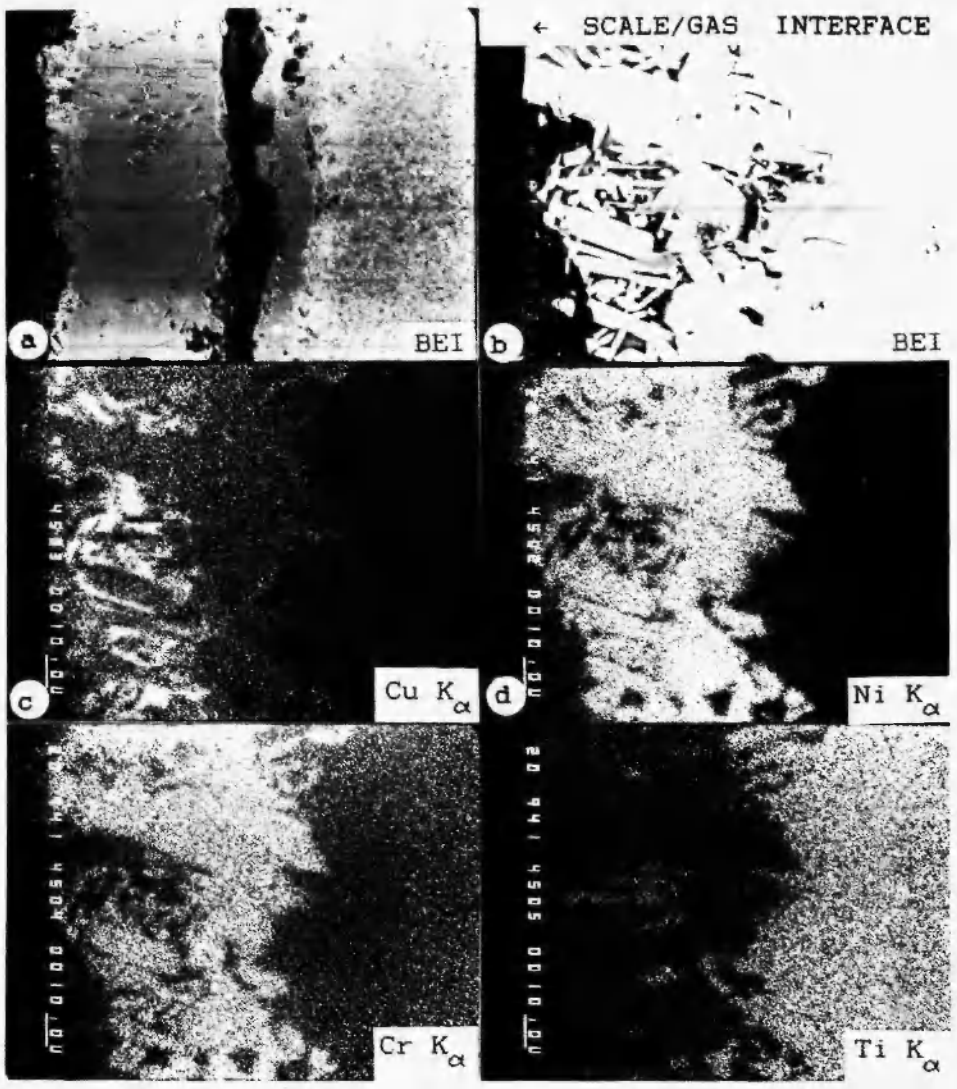

Fig. 9: The scale/gas interface in the (Ti, Cr)B_2-Cu-Ni alloy (1200°C, 6 hr); a – structure (secondary electrons); b – structure (backscattered electrons); c – Cu K_α; d – Ni K_α; e – Cr K_α; f – Ti K_α-radiation.

e). The intensity of Ti K_α-irradiation in these crystallites is close to that of the background (Fig. 9f). In accordance with the XRD and EPMA data, the inclusions with a higher copper content are Cu_2O oxide, light coloured crystallites are complex $CuCr_2O_4$ and $NiCr_2O_4$ oxides. Both the identical distribution of these elements and the similarity of $CuCr_2O_4$ and $NiCr_2O_4$ crystallographic structures lead to the conclusion that the formation of a (Ni, Cu)Cr_2O_4 solid solution takes place.

In this manner, impurities and alloying elements in both titanium diboride and in TiB_2-based alloys initially produce a diffusion barrier at the boride/scale interface. The formation of the first barrier is governed by values of Gibbs free energy for the appropriate oxides, whereas the formation of the second barrier is controlled mainly by the diffusion mechanisms for impurity cations. Impurities promote sintering of the scale. These factors increase the oxidation-resistance of titanium diboride with high impurity content and TiB_2-based alloys.

4.2.4. General regularities

By this means, during high-temperature oxidation

of titanium-based materials, the diffusion barrier is formed primarily at the matrix/scale (Fig. 10a). The diffusion barrier at the scale/gas is formed with time (Fig. 10b). The formation of the first diffusion barrier is determined principally by thermodynamics, i.e., by the initial formation of TiO_2 (rutile) scales. The formation of the second barrier is mainly determined by abnormally high diffusion rates of some impurity cations in rutile. There is no visible redistribution at the scale/scale interface in the two-layered scale (Fig. 10c). In such specific cases as the oxidation of titanium carbide and materials based on them, there are dispersed inclusions of oxidized binders or alloying elements in the inner scale (Fig. 10d). The distribution

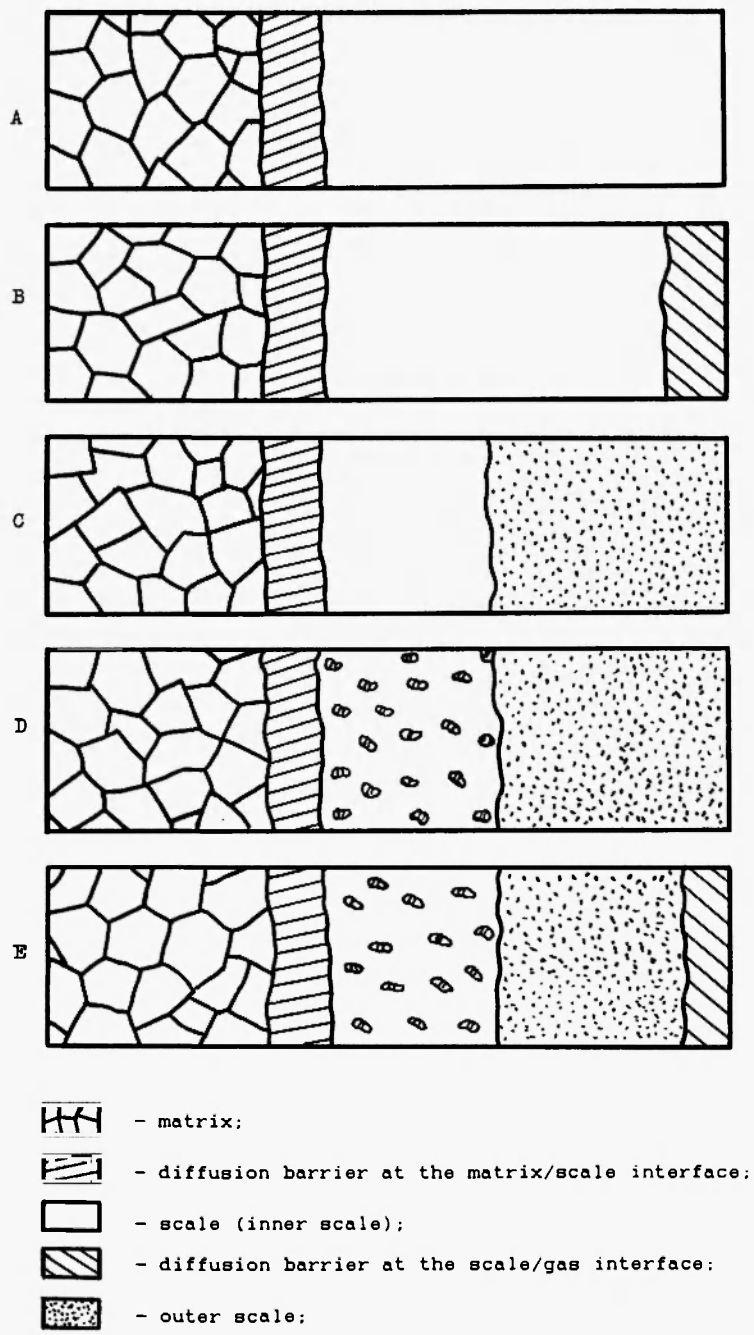

Fig. 10: Scheme of diffusion barriers formation in the TiO_2 (rutile) scales.

of elements is determined, in this case, by the features of the oxidation mechanism of these materials. The diffusion barrier at the outer scale/gas interface is formed with time, in accordance with the above mentioned regularities (Fig. 10e).

5. CONCLUSIONS

1. Mechanisms of distribution of elements both in the TiO_2 (rutile) scales and at the matrix/scale, scale/scale and scale/gas interfaces during high temperature oxidation of titanium-based materials, refractory compounds of titanium (carbide, diboride) and hard metals were investigated.
2. The diffusion processes of distribution of impurities and alloying elements in scales and at the interfaces are determined by the thermodynamics, oxidation mechanism, defect and crystallographic structure of rutile.
3. The distribution of elements and formation of diffusion barriers at the matrix/scale interfaces are determined by values of the Gibbs energy for oxide formation and oxidation mechanisms of metals, alloys and refractories. These factors determine the sequence of formation of appropriate oxides and the disposition of diffusion barriers in the subscale layers.
4. The distribution of elements at the inner scale and at the inner scale/outer scale interfaces is determined by the oxidation mechanism of the materials.
5. The distribution of elements in the outer scale and the formation of diffusion barriers at the scale/gas interface are determined by the peculiarities of defect and crystallographic structures of rutile. These factors cause fast diffusion of some impurity cations (Fe, Ni, Cr, Co, Cu) along channels of the rutile into the outer layers of the scale.

REFERENCES

1. A.I. Fromhold, *Theory of Metal Oxidation,, Vol. I, Fundamentals*, NHPC, Amsterdam, 1975; 547 pp.
2. R.F. Voitovich and E.I. Golovko, *High-Temperature Oxidation of Titanium and its Alloys*, Naukova Dumka, Kiev, 1984; 256 pp. [in Russian].
3. A.S. Bai, D.I. Lainer, E.N. Slesareva and M.I. Tsypin, *Oxidation of Titanium and its Allays*, Metallurgiya, Moscow, 1970, 317 pp. [in Russian].
4. P. Kofstad, *Nonstoichiometry, Diffusion and Electrical Conductivity in Binary Metal Oxides*, Mir, Moscow, 1975; 396 pp. [in Russian].
5. F. Millot, M.G. Blancin, R. Tetot, J.F. Marucco, B. Poumellec, C. Picard and B. Touzelin, *Progr. Solid State Chem.*, 17, 263 (1987).
6. E. Yagi, A. Koyama, H. Sakairi and R. Hasiguti, *J. Phys. Soc. Jap.*, **42**, 939 (1977).
7. H.B. Huntington and G.A. Sullivan, *Phys. Rev. Lett.*, **14**, A177 (1965).
8. J.P. Wittke, *J. Electrochem. Soc.*, **113**, 193 (1966).
9. R.D. Shannon and C.T. Prewitt, *Acta Cryst.*, **B25**, 925 (1969).
10. R.N. Blumental, J. Coburn and J. Bakus, *J. Phys. Chem. Solids*, **27**, 643 (1966).
11. J.F. Marucco, J. Cautron and P. Lemasson, *J. Phys. Chem. Solids*, **42**, 363 (1981).
12. P. Kofstad, *J. Less-Common Metals*, **13**, 635 (1967).
13. G. Levin and C. Rosa, *Z. Metallkunde*, **70**, 646 (1979).
14. K. Hoshino, N.L. Peterson and C.L. Wiley, *J. Phys. Chem. Solids*, **46**, 1397 (1985).
15. J. Sasaki, N.L. Peterson and K. Hoshino, *J. Phys. Chem. Solids*, **46**, 1267 (1985).
16. O.W. Jonson, *Phys. Rev.*, **136**, A284 (1964).
17. J.R. Akse and H.B. Whitehurst, *J. Phys. Chem. Solids*, **39**, 457 (1978).
18. M.F. Yan and W.W. Rhodes, *J. Appl. Phys.*, **53**, 8809 (1982).
19. J.F. Stebbins, I. Farnaan and V. Klabunde, *J. Amer. Ceram. Soc.*, 72, 2198 (1989).
20. E. Tani and F. Baumard, *J. Solid St. Chem.*, **32**, 105 (1980).
21. K.J.D. MacKenzie, *Trans. J. Br. Ceram. Soc.*, 74, 127 (1975).
22. E.A. Barringer and H.K. Bowen, *J. Amer. Ceram. Soc.*, **65**, C199 (1982).

23. M.F. Yan and W.W. Rhodes, *Mater. Sci. Eng.*, **61**, 59 (1983).
24. Y.K. Suyama and A. Kato, *Yohyo Kyokai Shi.*, 89, 140 (1981).
25. V. Schatt, K.P. Weiters and W. Rulle, *Powder Metall. Int.*, 17, 176 (1985).
26. V. Schatt, K.P. Weiters and W. Rulle, *Powder Metall. Int.*, 17, 232 (1985).
27. H.U. Anderson, *J. Amer. Ceram. Soc.*, **50**, 235 (1967).
28. D.J. Derry, D.G. Lees and J.M. Calvert, *J. Phys. Chem. Solids*, **42**, 57 (1981).
29. A.N. Bagshaw and B.G. Hyde, *J. Phys. Chem. Solids*, **37**, 835 (1976).
30. H.L. Schick, *Thermodynamics of Certain Refractory Compounds*, Academic Press, N.Y., 1966; Vol. 1 – 632 pp., Vol. 2 – 775 pp.
31. V.K. Grigorovich, in: *Theoretical and Experimental Methods of Investigation of Phase Diagrams of Metallic Systems*, Nauka, Moscow, 1969; p. 7 [in Russian].
32. J. Stringer, M.G. Cowgill and N.C. Griffith, *Nature*, **185**, 304 (1965).
33. A.M. Chaze, C. Goddet and G. Beranger, in: *Proc. 6th World Conference on Titanium*, Cannes, France, Les Editions de Physique, 1988; Vol. IV, p. 1765.
34. B. Champin, L. Graff and M. Armand, *J. Less-Common Metals*, 69, 169 (1980).
35. R. Tendler and J.P. Abriata, *J. Nucl. Mater.*, **150**, 251 (1987).
36. T.B. Massalski (ed.), *Binary Alloy Phase Diagrams*, American Society for Metals, Metals Park, Ohio, 1986; Vol. 1 – 1100 pp., Vol. 2 – 1124 pp.
37. V.K. Grigorovich, *Electron Structure and Thermodynamics of Iron Alloys*, Nauka, Moscow, 1970; 292 pp.
38. A. Takasaki, K. Ojima, Y. Taneda, T. Hoshiya and A. Mitsuhashi, *Scr. Metall. Mater.*, **27**, 401 (1992).
39. E.U. Lee and J. Waldman, *Scr. Metal.*, **22**, 1389 (1988).
40. Y. Umakoshi, M. Yamaguchi, T. Sakagame and T. Yamahe, *J. Mater. Sci.*, 24, 1599 (1989).
41. V.A. Tshai and P.V. Geld, *Phys. Metal. Metalloved.*, **16**, 495 (1963) [in Russian].
42. V.A. Gilyaev, V.D. Lubimov and G.P. Shveikin, *Izv. AN SSSR, Ser. Neorgan. Mater.*, **10**, 47 (1974) [in Russian].
43. V.A. Gilyaev, Yu.G. Zainullin, S.I. Alamovski and G.P. Shveikin, *Izv. AN SSSR, Ser. Neorgan. Mater.*, **12**, 2168 (1976) [in Russian].
44. P.V. Geld, in: *Carbides and Nitrides*, L. Taught (ed.), Mir, Moscow, 1974; p. 264 [in Russian].
45. P.V. Geld and V.A. Tshai, *Zhurn. Strukturn. Chimii.*, **5**, 235 (1964) [in Russian].
46. M. Reichle and J.J. Nickl, *J. Less-Common Metals*, **27**, 213 (1972).
47. R.F. Voitovich, *Oxidation of Carbides and Nitrides*, Naukova Dumka, Kiev, 1981; 192 pp. [in Russian].
48. V.B. Voitovich, E.I. Golovko, V.A. Tsyban, R.F. Voitovich and L.N. Beloborodov, in: *Proc. Powder Metallurgy World Congress PM-94, Vol. 1, Hard Materials.* Editions de Physique, Paris, 1994; p. 187.
49. D.F. Chun, D.Y. Kim and K.Y. Eun, *J. Amer. Ceram. Soc.*, **76**, 2049 (1993).
50. A. Lebugle and G. Montel, *Rev. Int. Hautes Temp. Refract.*, **11**, 231, (1974).
51. A. Tampieri and A. Bellosi, *J. Mater. Sci.*, 28, 649 (1993).
52. J.D. Katz, R.D. Blake and C.P. Scherer, *Ceram. Eng. Sci. Proc.*, **10**, 854 (1989).
53. V. Svistunov, A. Beketov, E. Knyshev, N. Obabkov and V. Novgorodtsev, *J. Less-Common Metals*, **67**, 287 (1979).
54. V.B. Voitovich, V.A. Lavrenko and V.M. Adejev, *Oxid. Met.*, **42**, 145 (1994).